

promoting access to White Rose research papers



Universities of Leeds, Sheffield and York
<http://eprints.whiterose.ac.uk/>

This is the published version of an article in the **Journal of Atmospheric and Oceanic Technology**, **20 (8)**

White Rose Research Online URL for this paper:

<http://eprints.whiterose.ac.uk/id/eprint/77231>

Published article:

Brooks, IM (2003) *Finding Boundary Layer Top: Application of a Wavelet Covariance Transform to Lidar Backscatter Profiles*. *Journal of Atmospheric and Oceanic Technology*, 20 (8). 1092 - 1105. ISSN 0739-0572

[http://dx.doi.org/10.1175/1520-0426\(2003\)020%3C109...](http://dx.doi.org/10.1175/1520-0426(2003)020%3C109...)

Finding Boundary Layer Top: Application of a Wavelet Covariance Transform to Lidar Backscatter Profiles

IAN M. BROOKS

University of Leeds, Leeds, United Kingdom

(Manuscript received 14 August 2002, in final form 7 February 2003)

ABSTRACT

Several recent studies have utilized a Haar wavelet covariance transform to provide automated detection of the boundary layer top from lidar backscatter profiles by locating the maximum in the covariance profiles. This approach is effective where the vertical gradient in the backscatter is small within and above the boundary layer, and where the inversion is sharp and well defined. These near-ideal conditions are often not met, particularly under stable stratification where the inversion may be deep and is sometimes ill defined, and vertical gradients are common. Here the effects of vertical gradients and inversion depth on the covariance transform are examined. It is found that a significant dilation-dependent bias in the determination of the boundary layer top may result when using the published method. An alternative approach is developed utilizing multiple wavelet dilations, and is capable of identifying both the upper and lower limits of the backscatter transition zone associated with the inversion while remaining insensitive to mean vertical gradients in the background signal. This approach enables more detailed information on the small-scale structure of the inversion and entrainment zone to be retrieved than is possible using existing techniques.

1. Introduction

Remote sensing techniques such as lidar and sodar are invaluable for the measurement of boundary layer (BL) properties that are difficult, or impossible, to measure directly at sufficient spatial or temporal resolution, over long periods, or with large areal coverage—for example boundary layer depth and entrainment zone structure. Lidar systems, in particular, have been widely used to examine the structure and variability of the BL top and to derive the entrainment zone depth (Boers et al. 1984; Nelson et al. 1989; Melfi et al. 1985; Flamant et al. 1997; Davis et al. 1997; Russell et al. 1998; Kiemle et al. 1998; Högeli et al. 2000; Cohn and Angevine 2000). The volume of data generated by lidar systems is substantial and automated processing is essential if full use is to be made of all the information available. Developing robust algorithms for extracting the information of interest—typically the altitude of the BL top—can be challenging, particularly where conditions depart from the ideal of a well-mixed BL capped by a sharp, well-defined inversion.

Lidar systems measure the intensity of backscattered light as a function of distance from the instrument. The primary contribution to scattering is from aerosol par-

ticles suspended in the air; at short wavelengths there may also be a nonnegligible contribution from molecular backscatter (Dupont et al. 1994). The atmospheric boundary layer typically has a much higher concentration of aerosol than the free troposphere above and thus provides a stronger backscatter signal; the substantial change in backscatter across the top of the BL provides a convenient means of determining the local BL depth. It is worth noting here that while the transition in lidar backscatter from BL to free-troposphere values is usually assumed to correspond closely with the temperature inversion, it does not respond directly to the thermodynamic properties of the atmosphere. In the discussion that follows we will thus refer to the region of high vertical gradient in lidar backscatter as the *transition zone*, although it is understood that for most applications this can be assumed to be a proxy for the temperature inversion. The word *inversion* will be reserved for the true temperature inversion.

Early lidar studies of entrainment zone structure used subjective visual estimates of the mean properties of the boundary layer top to define an entrainment zone (Boers et al. 1984; Nelson et al. 1989). Automated approaches have included the use of simple signal threshold values (Melfi et al. 1985; Boers et al. 1988), and identification of the minimum in the vertical gradient of the backscatter (Flamant et al. 1997). The first of these suffers from the need to define appropriate threshold values—a particular problem if the signal strength varies within

Corresponding author address: Dr. Ian Brooks, Institute for Atmospheric Science, School of the Environment, University of Leeds, Leeds LS2 9JT, United Kingdom.
E-mail: ibrooks@env.leeds.ac.uk

the dataset or if there is significant noise in the signal. The gradient approach also suffers from the effects of noise and small-scale structure in the backscatter profiles; these may produce large gradients unrelated to the large-scale BL structure. Filtering or averaging of the backscatter signal can minimize this problem but inevitably also degrades the part of the signal of interest. Steyn et al. (1999) developed an approach that utilizes the whole backscatter profile rather than just localized structures by fitting a well-defined idealized profile to the data and using this fitted function to define both the BL top and a local entrainment zone depth for each profile; however, Hägeli et al. (2000) found that while it was effective for well-mixed cases, it produced “quantitatively unrealistic” results for some more complex backscatter profiles. Several recent studies (Davis et al. 1997; Russell et al. 1998; Cohn and Angevine 2000) have utilized a wavelet-based technique, using a Haar function to provide a scale-dependent approach while retaining all of the information in the original backscatter profile. Cohn and Angevine (2000) and Davis et al. (2000) discuss the approach in some detail and describe its use for the determination of the BL depth for the case of a well-mixed, convective BL. Both consider, in a qualitative fashion the bias introduced by gradients in the background signal; Davis et al. (2000) also examine some more complicated cases: a multi-layered smoke plume and low signal-to-noise ratio. Here we consider in detail the complications and limitations arising from the effects of significant vertical gradients in backscatter and the substantial depth of the transition zone when applying this approach to lidar observations of the stable marine atmospheric boundary layer under cloud-free conditions. An alternative algorithm is developed that both circumvents the problems of the existing method and provides estimates of the limits of the transition zone.

2. The wavelet covariance transform

The wavelet covariance transform was defined by Gamage and Hagelberg (1993) as a means of detecting step changes in a signal. It is based upon a compound step function, the Haar function h , defined as

$$h\left(\frac{z-b}{a}\right) = \begin{cases} +1: & b - \frac{a}{2} \leq z \leq b \\ -1: & b \leq z \leq b + \frac{a}{2} \\ 0: & \text{elsewhere,} \end{cases} \quad (1)$$

where z is altitude, b is the location at which the Haar function is centered—the *translation* of the function, and a is the spatial extent, or *dilation*, of the function. The covariance transform of the Haar function, W_f , is defined as

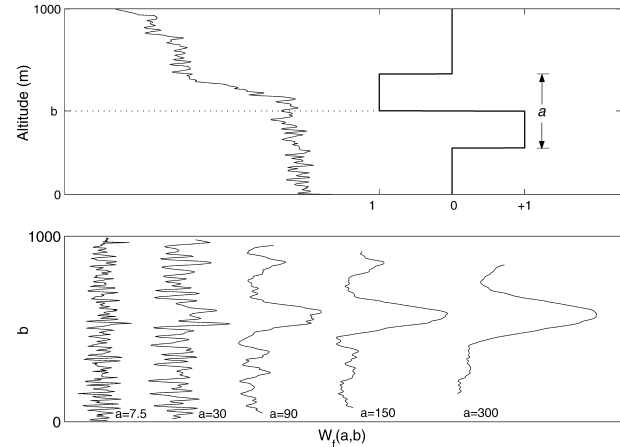


FIG. 1. An example of (top) a lidar backscatter profile and Haar function and (bottom) the resulting covariance transform at various values of the dilation [after Davis et al. (2000)].

$$W_f(a, b) = \frac{1}{a} \int_{z_b}^{z_t} f(z) h\left(\frac{z-b}{a}\right) dz, \quad (2)$$

where $f(z)$ is the signal of interest, in our case a lidar backscatter profile, and z_b and z_t are the lower and upper limits of the profile. A local maximum in $W_f(a, b)$ identifies a step in $f(z)$ with a coherent scale of a , located at $z = b$ (Fig. 1). The key to identifying features of interest is the selection of an appropriate dilation a ; Davis et al. (2000) show that for the simple case where the mean backscatter is near constant both within and above the BL, the choice of a is not crucial, provided it is large enough to distinguish the transition zone from small-scale variability in the signal. Under less ideal conditions the choice of dilation becomes important. A mean gradient in backscatter encompassing the entire wavelet results in a constant, nonzero value for $W_f(a, b)$; if the gradient is localized and coincides with only part of the wavelet, then it will contribute to $W_f(a, b)$ in proportion to the extent of the overlap. Cohn and Angevine (2000) demonstrated how a gradient in backscatter in the free troposphere results in an overestimate of the boundary layer depth determined from the maximum in $W_f(a, b)$ and suggested that this might explain an observed bias in their estimates of the inversion height during the early morning, when the convective BL was shallow and overlaid by a residual layer from the previous day. Davis et al. (2000) also found that the location of the maximum in $W_f(a, b)$ tended to increase with the dilation when a gradient in backscatter existed above the BL, but did not examine the behavior or implications for automated detection algorithms in detail.

The identification of BL depth from the location of the maximum in $W_f(a, b)$ works well where background gradients are negligible and the transition zone sharp and well defined, but these conditions are frequently not met. Under stable conditions, where mixing is poor, vertical gradients are common both within and above the

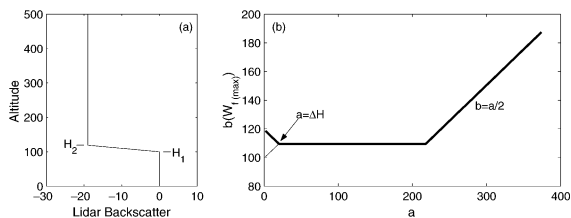


FIG. 2. (a) Idealized profile of the simplest case, where there is a vertical gradient only across the transition zone. (b) The location of the maximum in the wavelet covariance, $b[W_{f(\max)}]$, plotted against wavelet dilation a . For $a < (H_2 - H_1)$ there are multiple locations: the upper and lower limits only are indicated.

BL, and the inversion layer may be a significant fraction of the depth of the BL as a whole (Söderberg and Tjernström 2001); here the problem of identifying the BL depth in an automated manner becomes more complicated. It should also be noted that under some conditions the boundary layer may be so ill-defined that an absolute top cannot sensibly be defined.

Before we consider the effects of vertical gradients, it is worth noting some fundamental constraints on the useful values of the dilation and translation. Any real lidar profile is finite in length; useful values of a and b are thus limited to combinations for which the entire nonzero portion of the Haar function lies within the altitude range of the backscatter profile; outside of these limits part of the integral is undefined. The closest b may approach to the ends of the profile is thus $a/2$. The absolute maximum value of a is equal to the length of the measured profile; however, this extreme is of no practical use since b is then constrained to a single value of $a/2$. In practice the upper limit to the useful range of dilations is about twice the distance from the transition zone to the nearest end of the measured profile; at greater dilations the wavelet cannot be translated to a position at which its midpoint, b , coincides with the top of the BL.

3. The effect of vertical gradients

a. Theoretical treatment

Vertical gradients in the lidar backscatter result in a more complex problem in identifying the BL top because the location of the maximum in the covariance transform becomes dependent on the value of a . In all real data we expect to observe a vertical gradient in backscatter across the inversion since even for well-mixed convective conditions the inversion has a finite, if small, depth. Figure 2 shows an idealized backscatter profile with the transition zone base at H_1 and its top at H_2 , and the location of the maximum in $W_f(a, b)$ as a increases. For $a < (H_2 - H_1)$ there are multiple values of b for which $W_f(a, b)$ has the same (maximum) value; this is the region where the wavelet is entirely encompassed by the transition zone; only the extremes are shown here. As a approaches $(H_2 - H_1)$ the range of

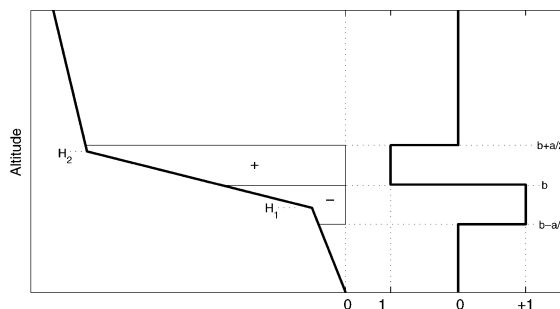


FIG. 3. Schematic figure of a generic lidar backscatter profile and Haar function. The integral in (2) is equal to the sum of the areas marked, where the contribution is positive/negative as indicated.

values narrows, converging on the midpoint of the transition zone, which remains a unique solution for all larger values of a up to $(H_2 + H_1)$. At this point the translation of the Haar function is limited by the bottom of the profile; if a is increased further, the maximum in $W_f(a, b)$ occurs when b is as low as possible, and $b[W_{f(\max)}] = a/2$. For this case—an idealization of a well-mixed BL with constant backscatter above the transition zone—the choice of dilation is not critical provided it lies within the limits $(H_2 - H_1) \leq a \leq (H_2 + H_1)$.

Consider the more general case where there are gradients in backscatter above and below the transition zone, as well as across it (Fig. 3). An analytical solution can be derived easily for our idealized profile, since the product of the backscatter profile and the Haar function amounts to the summation of the areas between the profile and an arbitrary zero line, here set at the base of the profile for convenience. The translation that gives a maximum in $W_f(a, b)$ for any given dilation can then be found by differentiating the expression for $W_f(a, b)$ with respect to b and solving for zero (for our idealized profile there is no minimum in the $W_f(a, b)$ profile, only a single maximum). For consistency throughout the discussion we set the height of the transition zone base and top as H_1 and H_2 , and the gradients, df/dz , below, across, and above the transition zone as G_1 , G_2 , G_3 , respectively. We assume that all three gradients are negative and that G_2 always has the largest magnitude, since that is the most commonly observed situation in the BL. We initially limit the range of values of b to between H_1 and H_2 , since we are only interested in identifying the height of the transition zone, and the dilation to $a \geq (H_2 - H_1)$. In this manner we find

$$b[W_{f(\max)}] = \frac{\frac{a}{2}(G_3 - G_1) + H_2(G_2 - G_3) + H_2(G_2 - G_1)}{(2G_2 - G_3 - G_1)}. \quad (3)$$

Figure 4 shows the results for several cases: artificial profiles were constructed with $H_1 = 100$, $H_2 = 119$, $G_2 = -1$, and G_1 and G_3 taking the values indicated in the

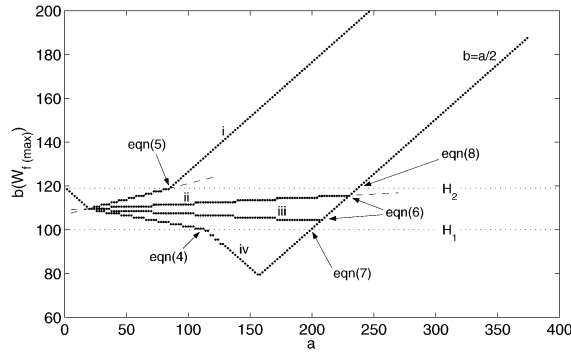


FIG. 4. The dotted lines show the values of $b[W_{f(\max)}]$ plotted against wavelet dilation a for discrete idealized profiles with $H_1 = 100$ m, $H_2 = 119$ m, $G_2 = -1$, and the following gradients within and above the BL: (i) $G_1 = -0.1$, $G_3 = -0.5$; (ii) $G_1 = -0.1$, $G_3 = -0.2$; (iii) $G_1 = -0.2$, $G_3 = -0.1$; (iv) $G_1 = -0.4$, $G_3 = -0.1$. Each dot represents a single result. The intercepts with the lines $b = H_1$, $b = H_2$, and $b = a/2$ are indicated along with the numbers of the equations that define them. The analytical solution for cases (i) and (ii) are shown as dashed lines (extended beyond their range of validity for clarity). The steps in the plotted lines are due to the discrete intervals between data points in the artificial profiles. For $a < \Delta H$ only the upper limit of the range of values for $b[W_{f(\max)}]$ is shown.

figure. The scale is arbitrary, but the artificial profiles were defined such that the number of points lying within the transition zone is of the same order as that observed for the lidar data examined below, thus providing a comparable degree of discretization. The locations of $b[W_{f(\max)}]$ as found by a wavelet covariance transform applied to the artificial profiles are shown individually as dots, while examples of the analytical expression (3) are shown as dashed lines. Note that (3) only applies for a limited range of dilations, defined below, but the line is extended in the figure for clarity. Several important points arise from (3) and Fig. 4. The value of $b[W_{f(\max)}]$ is clearly dependent upon the dilation, the depth of the transition zone, and the gradients above and below it. In general the midpoint of the transition zone is detected only when $a = (H_2 - H_1)$; the exception is when $G_1 = G_3$ in which case the behavior becomes identical to that in Fig. 2. Where G_1 and G_3 are unequal, $b[W_{f(\max)}]$ is pulled below or above the midpoint depending upon whether G_1 or G_3 is greater, and as the dilation is increased will eventually reach the lower or upper limit of the transition zone. The dilation for which $b[W_{f(\max)}] = H_1$ can be found by substitution in (3) to be

$$a = 2(H_1 - H_2) \frac{(G_2 - G_3)}{(G_3 - G_1)}. \quad (4)$$

Similarly the dilation for which $b[W_{f(\max)}] = H_2$ is

$$a = 2(H_2 - H_1) \frac{(G_2 - G_1)}{(G_3 - G_1)}. \quad (5)$$

For dilations larger than the limiting values in (4) or (5), $b[W_{f(\max)}]$ is found to decrease/increase as a function of $a/2$. For any profile of finite length, the limit on possible values of b imposed by the end of the profile

will eventually be reached; if the end is sufficiently close to the transition zone, this may occur while $H_1 \leq b[W_{f(\max)}] \leq H_2$. For the case where the bottom of the profile is closest, this occurs when

$$a = H_2 + H_1 \frac{(G_2 - G_1)}{(G_2 - G_3)}; \quad (6)$$

for larger dilations, $b[W_{f(\max)}] = a/2$ and no information is obtained about the backscatter profile. The transition between (4) and (6) occurs when $b[W_{f(\max)}] = a/2 = H_1$, and thus for

$$\frac{H_1}{H_2} = \frac{(G_3 - G_2)}{(2G_3 - G_1 - G_2)}, \quad (7)$$

and the transition between (5) and (6) when $b[W_{f(\max)}] = a/2 = H_2$; thus

$$\frac{H_1}{H_2} = \frac{(G_2 - G_3)}{(G_2 - G_1)}. \quad (8)$$

Although we expect an inversion and a transition zone of finite thickness for any real boundary layer, for the sake of completeness we will consider the case of an instantaneous jump of Δf across an infinitely thin inversion located at an altitude H , with gradients in f of G_1 and G_3 below and above the interface. We adopt a similar approach to that above; first consider the case where $|G_3| > |G_1|$; for some arbitrarily large dilation we expect $b[W_{f(\max)}]$ to lie above H , and obtain

$$b[W_{f(\max)}] = H + \frac{a}{2} + \frac{\Delta f}{(G_1 - G_3)}. \quad (9)$$

The minimum possible value for $b[W_{f(\max)}]$ is H ; this will occur for dilations smaller than some limiting value, found from (9) when $b[W_{f(\max)}] = H$; thus,

$$a = \frac{2\Delta f}{(G_3 - G_1)}. \quad (10)$$

Similarly if $|G_1| > |G_3|$, then we get

$$b[W_{f(\max)}] = H - \frac{a}{2} + \frac{\Delta f}{(G_1 - G_3)}, \quad (11)$$

and a limiting dilation of

$$a = \frac{\Delta f}{(G_1 - G_3)}. \quad (12)$$

Equations (10) and (12) can also be derived as limiting cases of (4) and (5) by using the substitution $\Delta f = G_2(H_2 - H_1)$, which remains valid in the limit as $H_1 \rightarrow H_2$ and $G_2 \rightarrow \infty$. Figure 5 illustrates the relationships described by (9)–(12). In this case the choice of dilation is not critical provided it is less than the limiting value given by (10) or (12). This situation might apply where the transition zone depth is less than the lidar range resolution. For discrete data it is possible for the limiting dilation in (10) or (12) to be smaller than twice the range resolution of the lidar; in this instance a suffi-

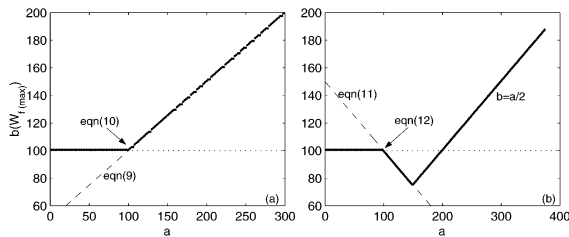


FIG. 5. The values of $b[W_{f(\max)}]$ plotted against wavelet dilation a for a backscatter profile with an infinitely thin transition zone: (a) $H = 100$, $G_1 = -0.1$, $G_3 = -0.3$, $df = -10$; (b) $H = 100$; $G_1 = -0.3$, $G_3 = -0.1$, $df = -10$. The analytical functions are plotted as dashed lines, and the equation numbers for these and the intercepts with $b = H$ are indicated.

ciently small wavelet cannot be constructed and $b[W_{f(\max)}]$ cannot be located directly.

b. Application to real data

The discussion above relates to highly idealized, smooth profiles; real lidar backscatter profiles exhibit both considerable small-scale structure caused by mixing and differential advection of air parcels, and random variability due to instrumental noise. Turbulence-scale atmospheric structures may change significantly over relatively short horizontal distances—potentially between consecutive lidar profiles; the large-scale structure, however, usually changes more gradually. The small-scale structure will lead to deviations from the idealized relationships above. If we consider the idealized cases to represent an ensemble mean of a set of backscatter profiles for which the large-scale structure changes little, then we might expect the results from individual profiles to scatter about the analytical expressions. Figure 6 shows a backscatter profile from the National Center for Atmospheric Research (NCAR) Scanning Aerosol Backscatter Lidar (SABL) flown on the NCAR C-130 Hercules during the Coastal Waves 96 (CW96) field campaign off the coast of northern California in June 1996 (Rogers et al. 1998). Figure 7 shows the location of the boundary layer top identified by the wavelet covariance transform plotted against the wavelet dilation along with the theoretical relation determined from (3) using values of H_1 , H_2 , and G_{1-3} estimated from Fig. 6. In order to ensure an equal number of points in both the positive and negative halves of the convolution, the wavelet is centered at the midpoint between lidar samples and the dilation is incremented at intervals of twice the lidar range resolution of 3.75 m. At the smallest dilations (7.5, 15, and 22.5 m) the transition zone is indistinguishable from small-scale structure and noise in the backscatter, and $b[W_{f(\max)}] \approx 99$ m (not shown); this corresponds to the upper edge of a prominent spike in the backscatter visible just below 100 m. As the dilation increases, the estimates of the boundary layer top scatter around the line predicted by (3). The range of values found is also

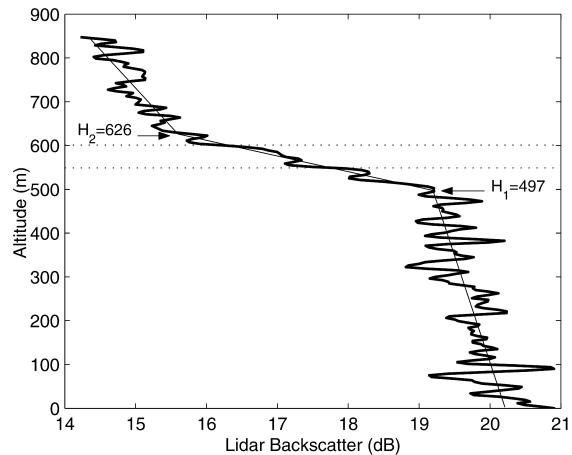


FIG. 6. A lidar backscatter profile from the CW96 project (heavy line). The bottom ($H_1 = 497$ m) and top ($H_2 = 626$ m) of the transition zone are approximate values selected by eye. The mean gradients $G_1 = -0.0021$, $G_2 = -0.028$, and $G_3 = -0.0057$ are overplotted as thin lines. The horizontal dotted lines at 601 and 549 m indicate the upper and lower limits of the BL top as detected by the wavelet covariance transform (see Fig. 7).

indicated in Fig. 6, note that, as predicted by the analytical treatment, all the values lie in the upper half of the transition zone. Points for $a > 500$ m can be neglected—these lie on a line decreasing with $a/2$; this is because the translation of the Haar function is limited to the top of the lidar profile, which is ≈ 250 m above the transition zone; the location of $b[W_{f(\max)}]$ is thus forced by the restrictions imposed upon the wavelet translation rather than the details of the lidar profile. The highest estimates of the BL top are obtained for $a < 120$ m; the estimated transition zone depth is about 129 m, so these are all instances where the entire wavelet can be encompassed by the transition zone. For the idealized case we found $b[W_{f(\max)}]$ to have multiple values with the uppermost increasing toward H_2 as a decreases from ΔH . In practice the small-scale structure in the backscatter provides a single value for $b[W_{f(\max)}]$; the precise value depends strongly on the details of that structure.

4. Finding the transition zone limits

a. Deep transition zones

So far we have focused on finding a single representative value of the boundary layer depth from a backscatter profile; where there are significant vertical gradients or a deep inversion there are substantial difficulties in unambiguously identifying such a value from a maximum in the covariance transform. It is also debatable where, within a deep inversion, one should try and locate a single value for the BL top. Of more practical use would be the identification of the upper and lower limits of the transition zone between the BL and free-troposphere regions of the profile. Davis et al.

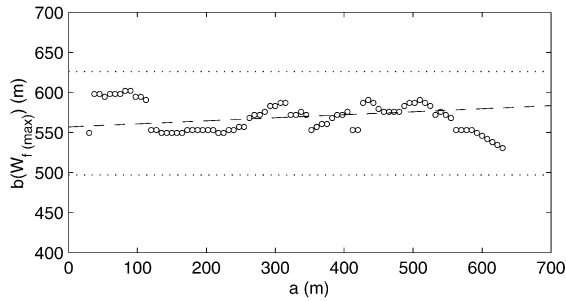


FIG. 7. The location of the BL top determined by the wavelet covariance transform plotted against wavelet dilation for the profile in Fig. 6. The three smallest dilations (7.5, 15, and 22.5 m) were insufficient to differentiate between the small-scale variability in the backscatter and identified the spike visible at approximately 100 m (points not shown). The dashed line is the relation given by (3); the horizontal dotted lines at 497 and 626 m indicate the approximate levels of H_1 and H_2 determined by eye.

(1997) noted that this transition zone may represent a more meaningful measure of the local entrainment zone depth than the commonly used area (or linear) averaged value obtained from the probability distribution of single BL top values (Nelson et al. 1989; Deardorff et al. 1980; Melfi et al. 1985). Kiemle et al. (1998) adopted such a local entrainment zone depth for a comparison of several BL regimes, identifying the upper and lower limits from predetermined threshold values of the backscatter.

Figure 8 shows profiles of $W_f(a, b)$ for the backscatter profile shown in Fig. 6, at various dilations between 7.5 m (the minimum possible) and 240 m. The dilation of 120 m is approximately equal to the transition zone depth and, thus, for an idealized backscatter profile

should have a maximum that provides the best estimate of the midpoint of the transition zone; Fig. 7 shows reasonable agreement with this ideal, at approximately 553 m. Secondary peaks just above and below the maximum show the influence of small-scale structure on $W_f(a, b)$. These peaks can be seen more clearly at smaller dilations where they are better defined. Each peak is located at close to the same level across all dilations, though the precise value varies slightly with dilation, and can be related back to features in the backscatter profile. Four such peaks are indicated in Fig. 8, at approximately 481, 514, 547, and 597 m (the values at $a = 30$ m). The lowest corresponds to the bottom of the transition zone, while the uppermost corresponds to its top. This suggests that the limits of the transition zone might be identified by examining $W_f(a, b)$ at small dilations. Note that neither of the peaks that correspond to the transition zone limits are necessarily the absolute maximum of $W_f(a, b)$ at any given dilation, and that for $a \leq 30$ m there is little difference in the size of the peaks of interest and those corresponding to other small-scale structures. In order to identify the relevant peaks we will make use the broad peak associated with the transition zone as a whole at larger dilations; the width of this peak is related to the depth of the transition zone and to the wavelet dilation as shown below, and can be used to define an envelope within which to search.

Consider the simple case of an idealized backscatter profile where $G_1 = G_3 = 0$, as shown in Fig. 9 [profile (i)] along with two corresponding profiles of $W_f(a, b)$ at dilations of 1 and 1.5 times the transition zone depth. We wish to identify H_1 and H_2 from $W_f(a, b)$. By determining the analytical expressions for $W_{f(\max)}$ and $W_f(b = H_{1,2})$ it can be shown that

$$\frac{W_f(b = H_{1,2})}{W_{f(\max)}} = \begin{cases} \frac{a - (H_2 - H_1)}{a - 1/2(H_2 - H_1)} & a \geq 2(H_2 - H_1) \\ \frac{a^2}{[4a - (H_2 - H_1)](H_2 - H_1)} & (H_2 - H_1) < a < 2(H_2 - H_1) \\ \frac{1}{2} & a \leq (H_2 - H_1). \end{cases} \quad (13)$$

The curve described by (13) is shown as the heavy solid line in Fig. 10a along with values calculated directly from $W_f(a, b)$ at $b = H_2$ for artificial backscatter profiles with various background gradients. For wavelet dilations less than the transition zone depth, $W_f(b = H_{1,2})$ is exactly half the maximum value of $W_f(a, b)$; this follows from the fact that $W_{f(\max)}$ occurs when the wavelet is completely encompassed by the transition zone gradient, while at $b = H_{1,2}$ just half of the wavelet coincides with the transition zone, the other half with a zero-gradient region above or below the transition zone.

As the dilation increases, the peak in $W_f(a, b)$ becomes broader and the ratio $W_f(b = H_{1,2})/W_{f(\max)}$ increases as the lines $b = H_{1,2}$ intersect $W_f(a, b)$ closer to its peak; this is demonstrated by the dashed curve in Fig. 9. Note that $W_f(a, b)$ is symmetric about the transition zone and thus the behavior at H_1 and H_2 is identical. When a gradient in backscatter exists above or below the transition zone, the $W_f(a, b)$ profile becomes asymmetric and the behavior at H_1 and H_2 differs, as shown by profile (ii) in Fig. 9; here $a = (H_2 - H_1)$ and the gradient affects $W_f(a, b)$ only at $b = H_2$. At larger dilations the

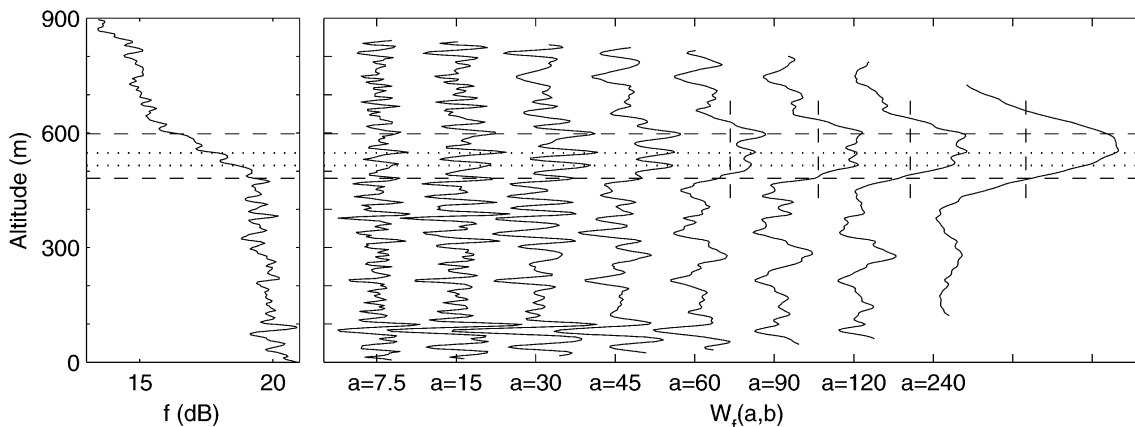


FIG. 8. The backscatter profile shown in Fig. 6, and profiles of $W_f(a, b)$ for the dilations indicated. Each profile is offset for clarity and its zero point indicated; the horizontal scale is the same for each profile, the absolute value is arbitrary; vertical dotted lines indicate $W_f(a, b) = 0.5W_{f(\max)}$ for the four largest dilations shown. The altitude of peaks in $W_f(a, b)$ corresponding to the structure within the transition zone are indicated by horizontal dotted lines at 481, 514, 547, and 597 m.

gradient affects $W_f(a, b)$ on both sides of the transition zone. Since the problem is essentially symmetric about the transition zone midpoint (it does not matter mathematically which end of the backscatter profile is which), we can deduce that the curves in Fig. 10a obtained for $b = H_1$ correspond to those for $b = H_2$ when the values of G_1 and G_3 are swapped. These results indicate that for a wavelet dilation of the order of the transition zone depth, $W_f(a, b)$ should have a value at $b = H_1$ or $b = H_2$ equal to, or greater than, half its maximum. Figure 10b shows how the width of the peak at half its maximum value varies with dilation for several combinations of gradients. The curves vary as a function of the ratio between G_2 and G_1, G_3 . Again, since it does not matter which end of the profile is which, G_1 and G_3 are interchangeable; any combination of $G_1,$

$G_2,$ and G_3 that maintains a constant ratio between them produces the same curve; increasing either G_1 or G_3 with respect to G_2 causes the peak width to increase at any given dilation, while decreasing the ratio causes the peak width to decrease. The curve for $G_1 = G_3 = 0$ is independent of the value of G_2 .

The $W_f(a, b)$ profiles shown in Fig. 8 are not quite so simple; the structure in the backscatter results in a significant departure from the idealized cases in Fig. 9. At the upper limit of the transition zone $W_f(a, b)$ is at or very close to its maximum value for all but the smallest dilations—larger than expected from the ideal case; consequently the location of $0.5W_{f(\max)}$ is higher than predicted. This might be explained by the presence of a significant gradient in backscatter above this level, but the discrepancy is larger than might be expected. At the

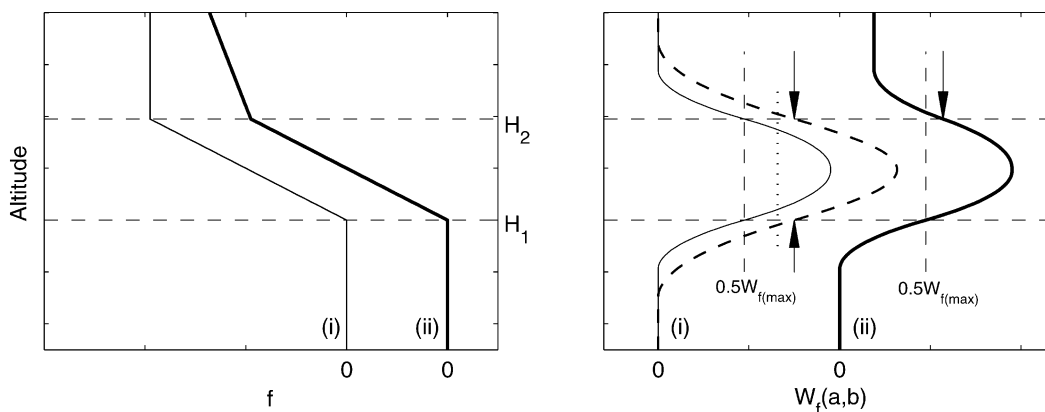


FIG. 9. (left) Idealized backscatter profiles with $G_1 = G_3 = 0$ [thin line, (i)] and $G_1 = 0, G_3 = -0.2$ [heavy line, (ii)]; $G_2 = -1$ in both cases. Profiles are offset for clarity. (right) Profiles of $W_f(a, b)$ for (i) with $a = H_2 - H_1$ (thin solid line) and $a = 1.5(H_2 - H_1)$ (heavy dashed line), and for (ii) with $a = H_2 - H_1$ (heavy solid line, profile offset for clarity). Here, $W_f = 0.5W_{f(\max)}$ is indicated by vertical dashed lines for both (i) and (ii) with $a = H_2 - H_1$, and by a vertical dotted line for (i) with $a = 1.5(H_2 - H_1)$. The altitudes of H_1 and H_2 are indicated by horizontal dashed lines in both panels. Arrows indicate the value of W_f at $b = H_2$ for (i) with $a = 1.5(H_2 - H_1)$ and (ii), where this differs from $0.5W_{f(\max)}$.

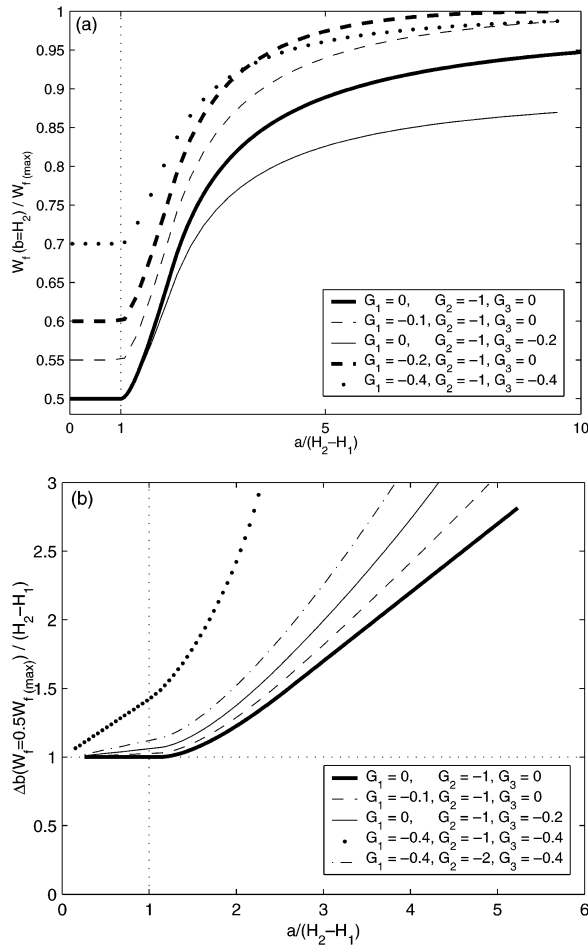


FIG. 10. (a) The ratio of $W_f(a, b)$ at $b = H_2$, the top of the transition zone, to its maximum value, as a function of $a/(H_2 - H_1)$. The heavy solid line is the analytical curve given by (13) for the case where $G_1 = G_3 = 0$. The other lines show the results calculated numerically from artificial profiles with the gradients shown in the figure legend. In all cases $G_2 = -1$, $H_1 = 200$, $H_2 = 239$. (b) The width of the peak in $W_f(a, b)$ at half its maximum value as a function of dilation, both normalized by the transition zone depth, for an idealized backscatter profile. Line types match those in (a) for the same conditions.

lower limit of the transition zone $W_f(a, b) < 0.5W_{f(\max)}$ at $b = H_1$ for $a = 60, 90$, and 120 m; the distortion is opposite to that expected: the broadening of the peak due to gradients above and below the transition zone should result in $W_f(a, b)$ having a higher value than for the ideal case. This asymmetry is found to be a general result for the CW96 dataset. It is a consequence of the mean shape of the backscatter profile in and around the transition zone; there is a tendency for the mean profile to be slightly convex (this is not obvious in Fig. 8, but see Fig. 15). This can be explained by considering the nature of the entrainment and mixing processes. Above the inversion, turbulent mixing is minimal or nonexistent; entrainment proceeds by the engulfment of an air parcel from immediately above the inversion, and its subsequent mixing into the boundary layer. The strength

of turbulence and the dominant eddy size both tend to increase with distance away from the boundary imposed by the inversion, thus scalar quantities such as water vapor or aerosol particles tend to have their maximum vertical gradients at the upper limit of turbulent mixing, and to decrease toward a more or less well-mixed condition within the main part of the boundary layer. Thus the scalar concentration profile tends to be more rounded on the boundary layer side of the inversion than on the free-troposphere side (see, e.g., Fig. 6.9 in Garratt 1992); this tendency is more pronounced when mixing is weak, as under stable conditions (e.g., Brooks and Rogers 2000, their Fig. 4). Figure 11 demonstrates the effect this curvature has on the $W_f(a, b)$ profile; the whole peak is pushed upward, skewing the values of $W_f(a, b)$ at H_1 and H_2 to lower and higher values, respectively. This effect combines with that of mean background gradients in backscatter, and local distortions due to small-scale structure, to produce profiles that depart significantly from the ideal.

In spite of this we can still make use of the result to define a reasonable range within which to search for the peaks in $W_f(a, b)$ for $a \ll H_2 - H_1$ that correspond to the transition zone, but must adopt an empirical approach to selecting reasonable limits. For H_1 we need to define a limit somewhat less than $0.5W_{f(\max)}$, while for H_2 a limit somewhat greater than $0.5W_{f(\max)}$ is required. Values of $0.7W_{f(\max)}$ and $0.3W_{f(\max)}$, respectively, have been found to work well with the lidar data obtained during CW96. The first peak in the covariance profiles at small dilations inside each of these limits identifies the extremes of the transition zone. These values were arrived at after several iterations of testing. Initial values were chosen based on an examination of several dozen backscatter profiles and their associated $W_f(a, b)$ profiles at various dilations, as in Fig. 8. The detection algorithm was then run for several thousand backscatter profiles drawn from several different days. The profiles and the estimated values of H_1 and H_2 were visually examined—particular attention was paid to all the profiles where the estimate of H_1 or H_2 differed significantly from neighboring profiles. Where the estimated transition zone limits differed from those identified by eye—usually due to small-scale structure above or below the limit being selected—the criteria were reevaluated and the entire process repeated.

Provided that $|G_2| \gg |G_1|$ or $|G_3|$ (a reasonable assumption for most BL lidar data), then the vertical gradient in $W_f(a, b)$ is large in the region of the limiting values chosen, and the distortion due to small-scale structure in the backscatter profiles does not cause a serious problem; the sensitivity to the size of dilation is also small so that the precise value of the dilation is not critical.

b. Shallow transition zones

The approach described above performs well where the transition zone depth is greater than the value of the

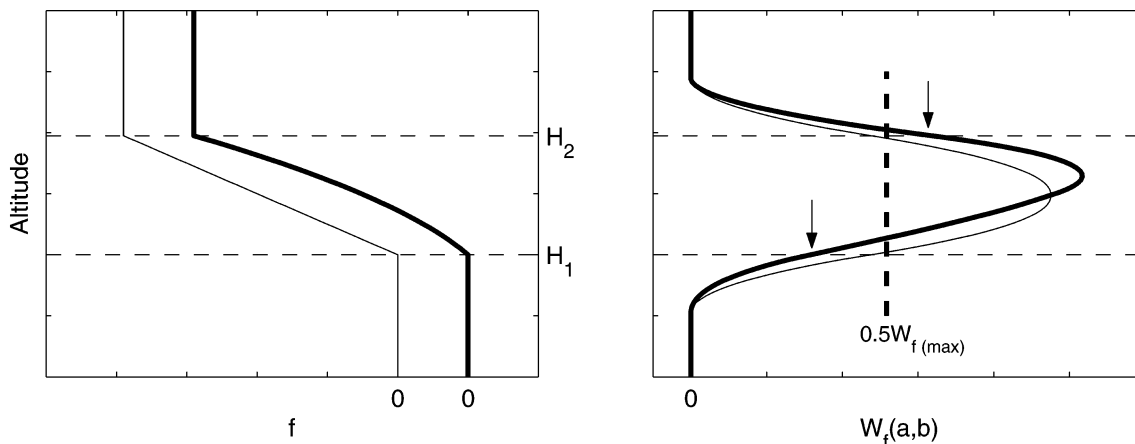


FIG. 11. Idealized profiles of lidar backscatter and $W_f(a, b)$ for linear (thin line) and convex (heavy line) transition zones, for $a = (H_2 - H_1)$. The heavy dashed line indicates $0.5W_{f(max)}$ for the convex transition zone case; arrows indicate the locations on the curve for $b = H_1$ and $b = H_2$.

small dilation employed; however, for depths smaller than this the wavelet can no longer resolve the transition zone limits reliably. We might consider using a smaller dilation still, if possible, but may then approach the limit imposed by the range resolution of the lidar and the effects of noise. We return instead to the relationship between peak-width and transition zone depth. At small dilations the peak associated with a shallow transition zone is well defined, and the departure from the ideal values of $W_f(a, b)$ at the transition zone limits, of half its maximum value, is minimal. Figure 12 shows the backscatter and wavelet covariance profile at $a = 30$ m for a case with a very shallow transition zone, approximately 26 m thick. The altitudes at which $W_f(a, b)$ is half its maximum value are indicated; these agree closely with the transition zone limits. Note that the peak is defined by a small number of data points, and in general the half-maximum location will lie between samples. We chose the first samples with values less than half the maximum as the locations of the transition zone

limits. This method works well for transition zone depths up to a limiting value of about twice the dominant scale of the small-scale structures, at which point the distortion of the $W_f(a, b)$ profile by the small-scale structures becomes significant.

Since the applicable ranges for the two approaches to identifying the transition zone limits overlap for transition zone depths between about 1 and 2 times the size of the smaller dilation, we choose to swap between approaches at the midpoint of the overlap, 1.5 times the minimum dilation. In practice the first approach is used for a first pass through the data, and the second approach then used for a second pass over any profiles for which the first pass found a transition zone depth less than this limit.

c. Dilation selection

The discussion above has dealt with the values of the wavelet dilations to be used only in very general terms.

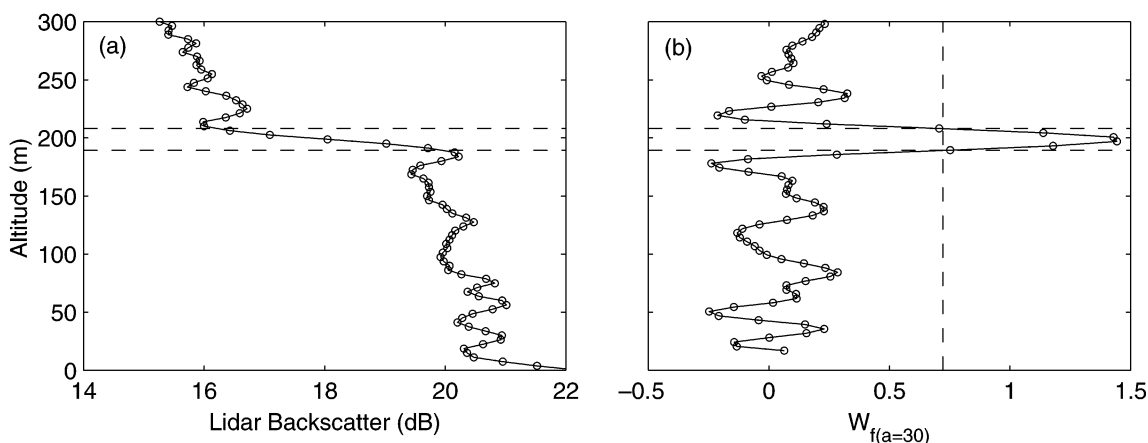


FIG. 12. (a) Backscatter profile and (b) wavelet covariance profile with a dilation of 30 m for a case with a very narrow transition zone. The locations at which $W_f(a, b)$ has half its maximum value are indicated by dashed lines.

The results shown in Fig. 10 suggest that a dilation of the order of the transition zone depth, or less, produces a peak width at half its maximum equal to or slightly larger than this depth. Larger dilations produce broader peaks. Since we do not know the transition zone depth in advance we cannot immediately select an appropriate dilation. For the idealized profiles we could simply start with a very small dilation, and this would give a good estimate of the transition zone depth immediately; however, for real profiles there is no way to identify which peaks are associated with the broad transition zone rather than small-scale structures at small dilations. We can make use of the general form of the curves in Fig. 10b to derive an estimate of width of the transition zone using an iterative approach. Start with an arbitrarily large dilation; assume it is larger than the transition zone width. The width of the peak in $W_f(a, b)$ produced will also be larger than the transition zone, by some unknown factor—the exact value will depend on both the dilation and the values of all three backscatter gradients, but is unimportant for our purpose. Assume some arbitrary factor of, say, 2 or 3 times the width of the transition zone; this provides a first estimate. The shape of the curves in Fig. 10 means that this value will be smaller than our initial guess, provided our assumed factor is large enough. Use this value as the dilation for the next iteration (note that for discrete data we will need to round our estimate to the nearest discrete dilation value), find the new peak width and again assume it is double or triple the transition zone width; this gives a second estimate. After a few iterations the estimates of transition zone depth should converge on a value close to the true depth; the discrepancy depends on the background gradients in backscatter, but is small where $|G_2| \gg |G_1|$ and $|G_3|$. If the estimates diverge, then the factor assumed as the ratio of peak width to transition zone depth is too small; repeat the process with a larger value. Note that while the final peak width approximates the transition zone depth, it does not necessarily represent the locations of H_1 and H_2 accurately.

In the case of real data there are some minor complicating factors. As the dilation employed decreases, multiple peaks may be resolved, some of which may be far from the transition zone; care must be taken to estimate the width of the peak associated with the transition zone only. This may be achieved by checking for consistency between successive iterations at decreasing dilations. Small-scale structure, noise, and any curvature of the backscatter profile across the transition zone all cause distortions from the ideal case. Thus the final estimate of the transition zone width is likely to differ from the true value; however, we use this value primarily to provide an optimum choice of dilation. Since the dependence of the peak width on dilation is small for values less than about double the transition zone depth, this discrepancy does not present a serious problem. In practice the range of transition zone depths over which a given dilation is effective is found to be quite broad:

a dilation of 120 m has proved effective for transition zones of between 40 and 200 m. This broad range results in part because, for a given dataset, the background gradients tend to vary little; thus, as the transition zone narrows, the ratio of G_2 to G_1 and G_3 increases, so the peak width at a given dilation decreases, partially compensating for the increase in the ratio of dilation to transition zone depth.

The small dilation required to identify the limits of a deep transition zone has an upper limit defined by the minimum scale of the structures resolved by the lidar, and a lower limit dependent on the scale and magnitude of instrumental noise. In order to determine an appropriate scale we must examine one or more sample backscatter profiles. Where instrumental noise is negligible, as in the SABL data presented here, it may be possible to estimate an appropriate scale by eye: from Fig. 6 we can easily see that the dominant small-scale structure has a vertical scale of between about 20 and 40 m. Examining the power spectra of profiles of either lidar backscatter or $W_f(a, b)$ provides a more objective approach. Figure 13a shows the power spectra of the backscatter profile from Fig. 6, truncated at 500 m so as to include only structure from within the BL and not the transition zone itself, which would contribute a large signal at long wavelengths. There is a prominent peak in the spectra at a wavelength of about 40 m. Figure 13b shows the spectra of $W_f(a, b)$ for the same portion of backscatter profile at the minimum possible dilation of 7.5 m, and at a dilation of 30 m; here the spectral peaks at about 30 and 40 m, respectively, are even more prominent. The lack of significant instrumental noise means that it would be possible here to use the smallest possible dilation to identify the limits of the transition zone; although better peak definition is achieved at the dilation close to the dominant scale of the structures. The effects of random noise are demonstrated in Figs. 13c and 13d; these show similar power spectra, but after white noise, with a variance of approximately half the change in backscatter across the transition zone, has been added to the initial backscatter profile. In the backscatter spectrum, there is a spectral gap separating the noise from the small-scale structure, which is thus still identifiable. The spectra of $W_f(a, b)$ at 7.5-m dilation displays a very narrow spectral gap, but the noise dominates the short-wavelength end of the spectra. This suggests that this dilation is too short to identify structure in the backscatter from the noise. At a dilation of 30 m the noise is partially filtered out; there is a distinct spectral gap, and the 30–40-m scale again displays the most prominent peak in the spectra; thus, the structure in the backscatter can be resolved from the noise at this dilation. Figure 14 shows part of the backscatter profile with noise added, and the $W_f(a, b)$ profiles with dilations of 7.5, 30, and 120 m. The conclusions drawn from the power spectra are confirmed: at the smallest dilation $W_f(a, b)$ is dominated by the white noise; at $a = 30$ the effects of the noise are visible in $W_f(a, b)$ but the peaks

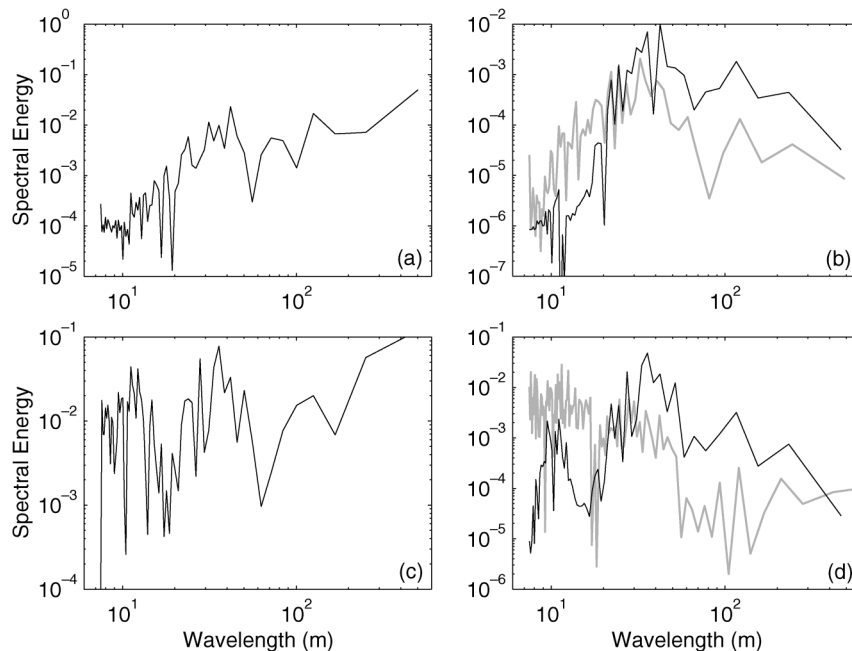


FIG. 13. Power spectra of (a) lowest 500 m of the backscatter profile from Fig. 6; (b) $W_f(a, b)$ profiles of lowest 500 m of the backscatter profile at dilations of 7.5 (gray line) and 30 m (black line); (c) same as in (a) but with white noise added to the backscatter profile; (d) same as in (b) but with white noise added to the backscatter profile.

associated with the small-scale structure are still clearly identifiable; at $a = 120$ the noise results in only minor distortions of the $W_f(a, b)$ profile.

Unlike the transition zone scale, this small-scale dilation should remain effectively constant for a given set of conditions (possibly even for a given instrument) and, thus, need only be determined once at the start of the analysis.

d. Algorithm summary

In the preceding sections we have developed techniques for estimating the upper and lower limits of the

transition zone in a lidar backscatter profile using information from a wavelet covariance transform at multiple wavelet dilations. These methods can be summarized as follows.

- 1) Examine power spectra of sample profiles of lidar backscatter and $W_f(a, b)$ to identify the minimum dilation a_1 capable of differentiating structure in the backscatter from random instrumental noise.
- 2) For each backscatter profile estimate an approximate transition zone depth via the iterative approach described in section 4c. This value gives the dilation a_2 for which the $W_f(a, b)$ profile is best suited to identifying the transition zone limits.

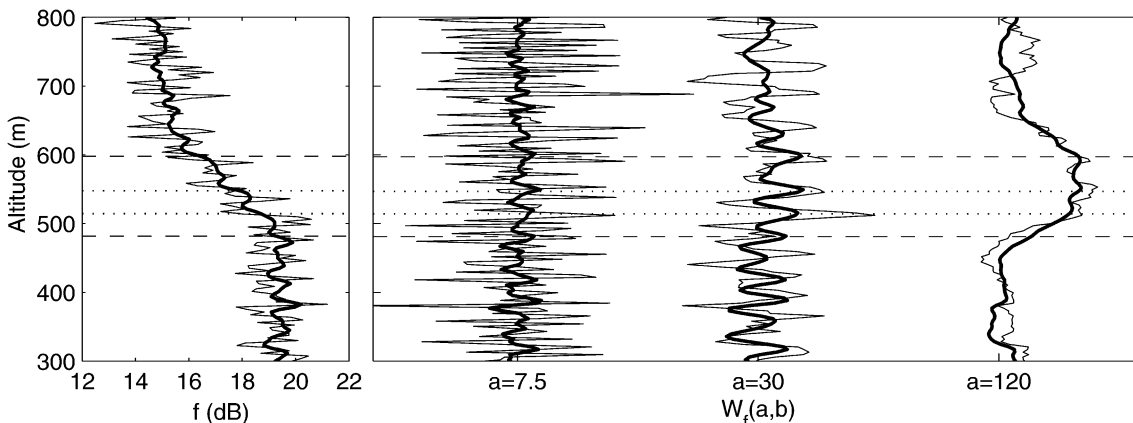


FIG. 14. Backscatter and selected $W_f(a, b)$ profiles from Fig. 8 (heavy lines) and with white noise added to the backscatter (thin lines).

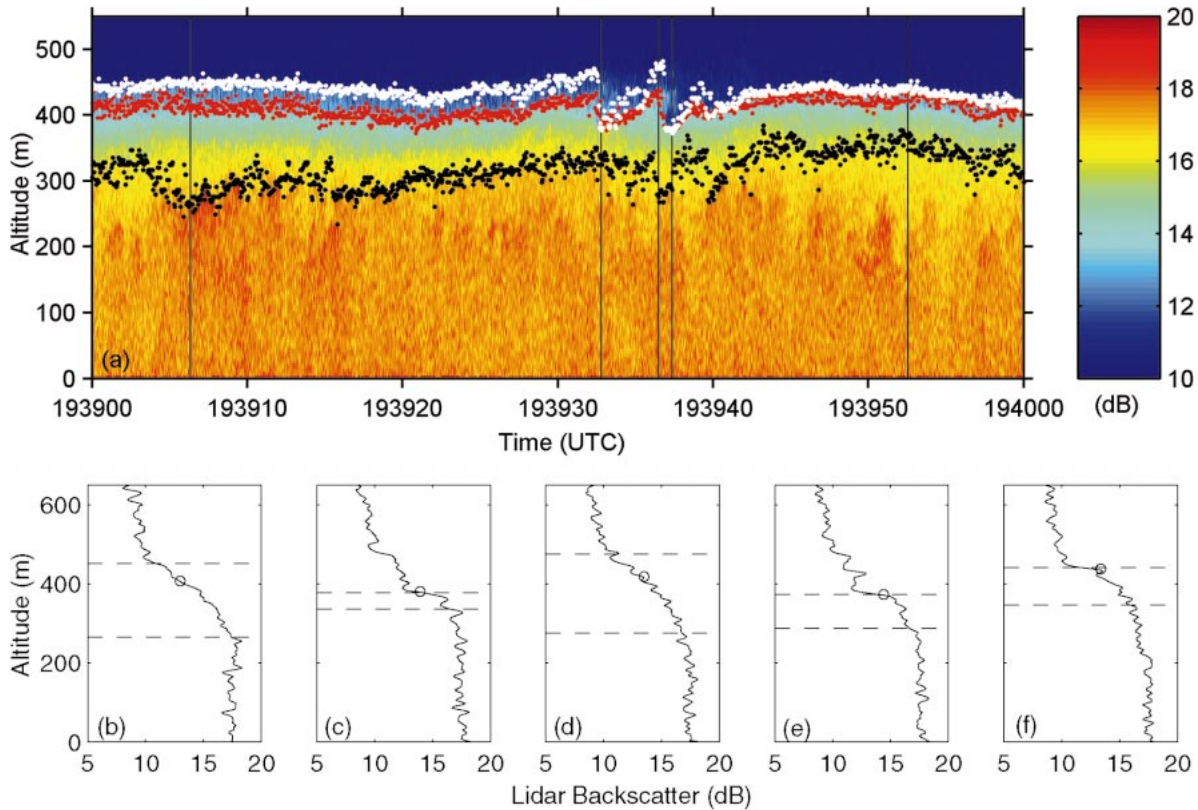


FIG. 15. (a) Lidar backscatter and the location of the transition zone base (black dots) and top (white dots) for a 6-km section of flight leg on 17 Jun 1996; red dots indicate the BL top as identified by the Davis et al. (2000) algorithm. (b)–(f) Individual backscatter profiles at each of the locations marked by vertical lines in (a) with the transition zone limits indicated by dashed lines; the Davis et al. algorithm results are indicated by circles. A breaking Kelvin–Helmholtz wave is visible between the times 1939:30 and 1939:40 UTC.

- 3) If $a_2 \leq 1.5a_1$, then the limits of the transition zone can be estimated directly as the locations at which $W_f(a, b)$ equals half its maximum value.
- 4) If $a_2 > 1.5a_1$, then find the locations at which $W_f(a, b)$ has values of 0.7 and 0.3 times its maximum on the upper and lower sides of the peak, respectively. The first peaks in $W_f(a_1, b)$ inside these limits provide good estimates of the locations of the upper and lower limits of the transition zone. If this results in $(H_2 - H_1) \leq 1.5a_1$, then use step 3 to make new estimates of H_1 and H_2 .

The methods described above have been tested on lidar data collected during CW96 within stable marine atmospheric boundary layers. A total of 121 990 individual profiles drawn from three different flights have been processed and the approach found to be highly effective. The processed data are being analyzed and will be presented in a future publication. Figure 15a shows an example of the data—a lidar backscatter cross section for a 6-km-long section of flight track on 17 June; there is a breaking Kelvin–Helmholtz wave visible between about 1939:30 and 1939:40 UTC. The locations of the transition zone base and top are marked for each of the 1200 backscatter profiles. Examples of individual

backscatter profiles, with a variety of transition zone structures, are shown in Figs. 15b–f. The locations of the BL top as identified by the Davis et al. (2000) algorithm are also shown for comparison; this successfully identifies the general location of the transition zone, but is biased toward the upper limit. The dilation used by Davis et al. is that which maximizes the function

$$D^2(a) = \int_{z_b}^{z_t} [W_f(a, b)]^2 db. \quad (14)$$

This is dependent upon the distance from the transition zone to the ends of the profile and, thus, on the arbitrary choice of exactly where the backscatter profile is truncated to remove the saturated signal in the near field. The tops of the backscatter profiles in Fig. 15a were truncated at 800 m; if the profiles are extended to 850 m, and the calculations repeated, the average BL top determined from the maximum in $W_f(a, b)$ at a dilation selected from the maximum in $D^2(a)$ increases by approximately 1.5 m; estimates for individual profiles change by up to 50 m. The determination of H_1 and H_2 relies entirely upon details of the backscatter in the vicinity of the transition zone and is thus independent of

arbitrary changes to the truncation of the ends of the profile.

e. Modifications, enhancements, and limitations

The methods described above should work well for a wide range of conditions; there are, however, a number of limitations. If the distance between one edge of the transition zone and the end of the profile is less than about half the transition zone depth, then the limit imposed upon the wavelet translation would prevent the identification of the transition zone edge. This problem could be circumvented by introducing a check on the distance to the end of the profile and adjusting the dilation used accordingly. The approach relies upon information derived from wavelets at dilations as small as possible; in cases where random noise was much greater than the signal from small-scale structures, it might fail completely. It would, however, remain possible to identify approximate locations of the transition zone limits directly from the width of the covariance peak for the large-dilation wavelet.

Davis et al. (2000) show how it is possible to identify the presence of multiple layers within the atmosphere. The methods developed here could be similarly adapted to identify different layers. For example, the $W_f(a, b)$ profiles at dilations of between 60 and 120 m in Fig. 8 show a distinct peak at an altitude of approximately 300 m. At smaller dilations this is lost among the peaks associated with the small-scale structures, while at large dilations it remains visible but becomes less well defined. This peak is associated with a small step in the backscatter profile: this represents the top of an internal boundary layer identifiable in profiles of virtual potential temperature and turbulence quantities made along the same ground track (not shown) and is a consistent feature in the lidar imagery for this day.

5. Conclusions

The effects of vertical gradients in lidar backscatter within and above the BL, and across the inversion, on the performance of a method described by Davis et al. (2000) for finding BL depth using a wavelet covariance transform have been examined. The method as implemented in previous studies (Davis et al. 1997; Russell et al. 1998; Cohn and Angevine 2000) utilizes only the maximum in the wavelet covariance and performs well when the vertical gradients in backscatter within and above the BL are small, and the transition zone is sharp and well defined. When the background gradients become large, a significant bias is introduced into the determination of the BL top; this bias is a function of wavelet dilation, the magnitude of the vertical gradients, and the thickness of the transition zone layer. It is not possible to quantify the bias, or to select the optimum wavelet dilation without a priori knowledge of the contributing factors. In many applications, particularly

where the inversion depth is substantial, the identification of a single estimate of its approximate level is not sufficient; more useful would be the identification of the upper and lower limits of the transition zone—the lower limit is of particular interest since it represents the top of the well mixed layer. It has also been noted that the depth of this transition layer between free-troposphere and boundary layer properties may be a better estimate of the local entrainment zone depth than the area-averaged value usually defined (Davis et al. 1997).

A method has been developed that utilizes information from the wavelet covariance transform at multiple dilations to identify the upper and lower limits of the transition zone. The method has been tested with lidar data collected during the CW96 field program within stable marine boundary layers, and appears robust, performing well for a wide range of both vertical gradients in backscatter and transition zone depths. This approach enables more detailed information on the structure and small-scale variability of the transition zone between the free troposphere and boundary layer to be retrieved, in a robust and objective manner, than has been possible using previous techniques. The limiting values employed were derived from a particular dataset and for a specific instrument. They are believed to be applicable to a wide variety of conditions for the SABL system, but may require adjusting for other instruments or for very different conditions. The basic approach, however, remains widely applicable. Although the development of this approach was prompted by the need to process lidar data from stable marine boundary layers, and its application has so far been limited to this dataset, it is applicable to a much wider range of conditions.

Acknowledgments. This work was supported by National Science Foundation Grant ATM-0100685 and Office of Naval Research Grant N00014-01-1-0258. The comments of three anonymous reviewers have contributed both to improvements in the manuscript, and the further development of the some of methods described.

REFERENCES

- Boers, R., E. W. Eloranta, and R. L. Coulter, 1984: Lidar observations of mixed layer dynamics: Tests of parameterized entrainment models of mixed layer growth rate. *J. Climate Appl. Meteor.*, **23**, 247–266.
- , J. D. Spinhirne, and W. D. Hart, 1988: Lidar observations of the fine-scale variability of marine stratocumulus clouds. *J. Appl. Meteor.*, **27**, 797–810.
- Brooks, I. M., and D. P. Rogers, 2000: Aircraft observations of the mean and turbulent structure of a shallow boundary layer over the Persian Gulf. *Bound.-Layer Meteor.*, **95**, 189–210.
- Cohn, S. A., and W. M. Angevine, 2000: Boundary-layer height and entrainment zone thickness measured by lidars and wind profiling radars. *J. Appl. Meteor.*, **39**, 1233–1247.
- Davis, K. J., D. H. Lenschow, S. P. Oncley, C. Kiemle, G. Ehret, and A. Giez, 1997: Role of entrainment in surface–atmosphere interactions over a boreal forest. *J. Geophys. Res.*, **102**, 29 219–29 230.
- , N. Gamage, C. R. Hagelberg, C. Kiemle, D. H. Lenschow, and

- P. P. Sullivan, 2000: An objective method for deriving atmospheric structure from airborne lidar observations. *J. Atmos. Oceanic Technol.*, **17**, 1455–1468.
- Deardorff, J. W., G. E. Willis, and B. H. Stockton, 1980: Laboratory studies of the entrainment zone of a convectively mixed layer. *J. Fluid Mech.*, **100**, 41–64.
- Dupont, E., J. Pelon, and C. Flamant, 1994: Study of the moist convective boundary-layer structure by backscatter lidar. *Bound-Layer Meteor.*, **69**, 1–25.
- Flamant, C., J. Pelon, P. H. Flamant, and P. Durand, 1997: Lidar determination of the entrainment zone thickness at the top of the unstable marine atmospheric boundary layer. *Bound-Layer Meteor.*, **83**, 247–284.
- Gamage, N., and C. Hagelberg, 1993: Detection and analysis of microfronts and associated coherent events using localized transforms. *J. Atmos. Sci.*, **50**, 750–756.
- Garratt, J. R., 1992: *The Atmospheric Boundary Layer*. Cambridge University Press, 316 pp.
- Hägeli, P., D. G. Steyn, and K. B. Strawbridge, 2000: Spatial and temporal variability of mixed-layer depth and entrainment zone thickness. *Bound-Layer Meteor.*, **97**, 47–71.
- Kiemle, C., G. Ehret, and K. J. Davis, 1998: Airborne lidar studies of the entrainment zone. *Proc. 19th Int. Conf. on Laser Radar*, Annapolis, MD, NASA, 395–398.
- Melfi, S. H., J. D. Sphinirne, S. H. Chou, and S. P. Palm, 1985: Lidar observations of the vertically organized convection in the planetary boundary layer over the ocean. *J. Climate Appl. Meteor.*, **24**, 806–821.
- Nelson, E., R. B. Stull, and E. Eloranta, 1989: A prognostic relationship for entrainment zone thickness. *J. Appl. Meteor.*, **28**, 885–903.
- Rogers, D. P., and Coauthors, 1998: Highlights of Coastal Waves 1996. *Bull. Amer. Meteor. Soc.*, **79**, 1307–1326.
- Russell, L. M., D. H. Lenschow, K. K. Laursen, P. B. Krummel, S. T. Siems, A. R. Bandy, D. C. Thompson, and T. S. Yates, 1998: Bidirectional mixing in an ACE 1 marine boundary layer overlain by a second turbulent layer. *J. Geophys. Res.*, **103**, 16 411–16 432.
- Söderberg, S., and M. Tjernström, 2001: Supercritical channel flow in the coastal atmospheric boundary layer: Idealized numerical simulations. *J. Geophys. Res.*, **106** (D16), 17 811–17 829.
- Steyn, D. G., M. Baldi, and R. M. Hoff, 1999: The detection of mixed layer depth and entrainment zone thickness from lidar backscatter profiles. *J. Atmos. Oceanic Technol.*, **16**, 953–959.